CHEMISTRY OF MATERIALS
Article

Chem. Mater. **2009,** *21,* 2705–2713 2705
DOI:10.1021/cm803310k

Preparation and Characterization of Glassy Carbon Powder Modified with a Thin Layer of Boron-Doped Ultrananocrystalline Diamond (B-UNCD)

Doo Young Kim,[†] Belabbes Merzougui,[‡] and Greg M. Swain*,[†]

[†]*Department of Chemistry and the Fraunhofer Center for Coatings and Laser Applications, Michigan State University, East Lansing, Michigan 48824-1322, and* [‡]*UTC Power Corporation, 195 Governors Highway, MS 601-19, South Windsor, Connecticut 06074*

Received January 13, 2009. Revised Manuscript Received April 6, 2009

The surface of glassy carbon powder (4 μm diam, 2 m^2/g) was modified with a thin layer of boron-doped ultrananocrystalline diamond (B-UNCD) for the purpose of improving the dimensional stability and corrosion resistance of the material. The UNCD layer was deposited by microwave-assisted chemical vapor deposition using a 1% CH_4, 7% H_2, 92% Ar and 1×10^{-3} % B_2H_6 (10 ppm) source gas mixture at 800 W of microwave powder and a system pressure of 140 Torr. Each sample was coated twice using a 2 h growth period with powder mixing in between to increase the number of particles coated and the coverage over each particle. SEM, XRD, Raman spectroscopy, and electrochemical methods were used to characterize the as received and B-UNCD-GC powders before and after anodic polarization at 1.6 V vs Ag/AgCl (25 °C, 30−60 min) in 0.5 M H_2SO_4. Most particle surfaces were coated with a thin layer of UNCD and there was some particle aggregation due to diamond overlayer formation over multiple neighboring particles. The results demonstrate that the as received powder undergoes surface oxide formation, layer plane exfoliation and fracturing caused by the stress of the oxide formed and or the oxidation of an intercalation compound, and carbon corrosion during electrochemical polarization. On the other hand, negligible microstructural damage or corrosion was found for the B-UNCD-coated powder. The work demonstrates that modification of sp^2 carbon powders with a thin layer of conducting diamond is a viable approach for creating a more durable and corrosion-resistant carbon powder.

Introduction

High-surface-area carbon powder (sp^2-bonded) is used as an electrocatalyst support in proton exchange membrane (PEM) fuel cells. The carbon is a key component of the all-important membrane electrode assembly (MEA), where the oxygen reduction and hydrogen oxidation reactions occur and electricity is produced. Structurally, the MEA is a complex material system comprised of a solid polymer electrolyte membrane as an electrolyte and porous carbon black supporting Pt electrocatalyst as the anode and cathode.[1] Improving the MEA stability is an important area of research these days because significant improvement in the durability is needed if PEM fuel cells are to find widespread application in transportation and stationary power. For example, lifetime targets are 5000 h for transportation and 40 000 h for stationary power, but these targets cannot be presently met because of material limitations.

Microstructural degradation and corrosion of the carbon electrocatalyst support is a critical hurdle to cross in order to achieve the targeted fuel cell lifetimes.[2−7] Carbon can undergo electrochemical oxidation during certain transient operations such as start-up/shut-down and local H_2 starvation.[1,3,6,8−10] Oxidation of the carbon can proceed in a stepwise manner that includes the formation of surface oxides with minimal microstructural damage, layer plane fracturing and exfoliation due to the stress induced by the surface oxides or oxidation of intercalation compounds, and corrosion. The overall carbon corrosion reaction ($E^o=0.207$ V vs SHE) is

$$C + 2H_2O \rightarrow CO_2 + 4H^+ + 4e^-$$

The electrochemical oxidation reaction mechanism and kinetics depend on the carbon microstructure (i.e., the

*Corresponding author.

(1) Liu, Z. Y.; Brady, B. K.; Carter, R. N.; Litteer, B.; Budinski, M.; Hyun, J. K.; Muller, D. A. *J. Electrochem. Soc.* **2008**, *155*, B979.
(2) Stevens, D. A.; Dahn, J. R. *J. Electrochem. Soc.* **2003**, *150*, A770.
(3) Paik, C. H.; Jarvi, T. D.; O'Grady, W. E. *Electrochem. Solid-State Lett.* **2004**, *7*, A82.
(4) Kangasniemi, K. H.; Condit, D. A.; Jarvi, T. D. *J. Electrochem. Soc.* **2004**, *151*, E125.
(5) Roen, L. M.; Paik, C. H.; Jarvi, T. D. *Electrochem. Solid-State Lett.* **2004**, *7*, A19.
(6) Stevens, D. A.; Hicks, M. T.; Haugen, G. M.; Dahn, J. R. *J. Electrochem. Soc.* **2005**, *152*, A2309.
(7) Reiser, C. A.; Bregoli, L.; Patterson, T. W.; Yi, J. S.; Yang, J. D.; Perry, M. L.; Jarvi, T. D. *Electrochem. Solid-State Lett.* **2005**, *8*, A273.
(8) Ferreira, P. J.; laa O', G. J.; Shao-Horn, Y.; Morgan, D.; Makharia, R.; Kocha, S.; Gasteiger, H. A. *J. Electrochem. Soc.* **2005**, *152*, A2256.
(9) Borup, R.; Meyers, J.; Pivovar, B.; Kim, Y. S..; et al. *Chem. Rev.* **2007**, *107*, 3904.
(10) Liu, Z. Y.; Brady, B. K.; Carter, R. N.; Litteer, B.; Budinski, M.; Hyun, J. K.; Muller, D. A. *J. Electrochem. Soc.* **2008**, *155*, B979.

Published on Web 06/17/2009

more microstructurally disordered the carbon, the more rapid the oxidation reaction kinetics), the anodic potential experienced, the pH, and the temperature. Even minor carbon oxidation can be deleterious in terms of reduced electrocatalytic activity and increased ohmic resistance within the electrode because of reduced catalyst−carbon and carbon particle−particle connectivity. The most catastrophic damage is caused by carbon corrosion or gasification. This causes permanent mass loss due to generated CO_2. As mentioned above, carbon corrosion is most problematic during start-up/shut-down and local H_2 starvation,[1,3,6,8−10] not during normal fuel cell operation. During these transient conditions, the cathode can briefly experience potentials as anodic as 1.4 V vs RHE. Advanced carbon materials are needed that undergo substantially less microstructural degradation and carbon corrosion at these potentials.

To this end, we have been investigating high surface area diamond powder[11−13] and diamond-coated sp^2 carbon materials[14] for their viability as dimensionally stable electrocatalyst supports. A significant body of work now exists confirming that boron-doped diamond, as well as the diamond-coated sp^2 carbons, exhibit superior dimensional stability and resistance to electrochemical oxidation as compared to sp^2 carbons.[11−18] For example, platinized diamond undergoes no observable microstructural damage, corrosion or lost catalytic activity during anodic polarization (2 h) in 85 wt % H_3PO_4 at 170 °C and 0.1 A/cm^2. In contrast, a platinized sp^2 carbon cloth degrades catastrophically within the first minutes of such a polarization.[17] We have also shown that conductive diamond powder is stable electrically and structurally during a 5 h polarization at 1.4 V vs RHE in 0.5 M H_2SO_4 at 80 °C [13].

Synthetic diamond is normally a superb electrical insulator; however, electrical conductivity can be imparted to the material through controlled doping with impurities, like boron. Long-term, we seek to develop high surface area (>100 m^2/g) and high electrical conductivity (1 S/cm) forms of diamond. This can be accomplished by overcoating small diamond powder particles with a thin layer of boron-doped diamond. To date, we have overcoated these powders with so-called microcrystalline diamond deposited from H_2-rich source gas mixtures[11,12] and so-called ultrananocrystalline diamond (UNCD) deposited from Ar-rich source gas mixtures[13]. Diamond abrasive powders are available commercially with diameters ranging from 3 nm up to 12 μm and are relatively inexpensive, costing as little as a few dollars per gram (e.g., detonation nanodiamond, >100 m^2/g). Using a core−shell approach, the powders are overcoated with a thin layer of boron-doped diamond[11−13]. The same approach has been used by John and co-workers to prepare diamond microshells[19,20]. In our work, individual particles are coated and aggregates are formed when multiple neighboring particles are covalently attached by the doped diamond overlayer[11−13]. UNCD seems to be the best synthetic form of diamond for coating these small, irregularly shaped objects. For example, the surface of Toray carbon paper has been modified with B-UNCD; a protocol that imparts a high degree of durability to this backing material.[14]

We show presently that a high degree of corrosion resistance can be imparted to sp^2 carbon powders by overcoating them with a thin layer of conducting diamond. Glassy carbon powder (4 μm diam., 2 m^2/g) was modified with a thin overlayer of boron-doped UNCD. The modified powders were characterized by scanning electron microscopy, X-ray diffraction, and Raman spectroscopy. The electrochemical properties were evaluated with the powder packed into a pipet electrode (binderless).[13] Finally, the dimensional stability and corrosion resistance were investigated during anodic polarization at 1.6 V vs Ag/AgCl (~1.8 V vs. RHE) for 1 h in 0.5 M H_2SO_4 at 80 °C.

Experimental Section

Boron-Doped Ultrananocrystalline Diamond Growth. An overlayer of boron-doped ultrananocrystalline diamond (B-UNCD) was grown on glassy carbon powder (Sigradur G, HTW GmBH, Germany) by microwave plasma-assisted chemical vapor deposition (CVD) (1.5 kW ASTeX, Inc., Lowell, MA). The glassy carbon powder was heat treated at 2000 °C, and had a nominal diameter of 4 μm and a specific surface area of 2 m^2/g. The modification first involved spreading a thin layer of the powder (approximately 30 mg) over the surface of a silicon wafer that was positioned in the CVD reactor. The powder was used as-received without any cleaning or seeding. The B-UNCD overlayer was deposited from an ultrahigh-purity $CH_4/H_2/Ar/B_2H_6$ source gas mixture consisting of 1% CH_4, 7% H_2, and 92% Ar. Ten parts per million (1×10^{-3} %) B_2H_6 was added for boron-doping, which imparts electrical conductivity to the diamond overlayer. The B-UNCD layer was deposited at 800 W of microwave power and 140 Torr. Typically, each glassy carbon powder sample was coated twice, and the growth period for each was 2 h. After the first growth, the GC powder sample was mixed and respread over the Si surface in order to enhance diamond growth on all areas of the powder surface. The two-growth procedure with mixing resulted in more complete coating of the powder surface. After each growth, a postgrowth annealing and cool-down procedure was employed to minimize the formation of adventitious sp^2 carbon impurity and to ensure maximum hydrogen surface termination. This procedure involved stopping the CH_4 and B_2H_6 gas flows, leaving the sample exposed to an H_2/Ar plasma for 10 min. The microwave power and pressure were then slowly reduced over 20-min period to 100 W and 50 Torr. This cooled the sample to less than 400 °C in the presence of a low level of atomic hydrogen, which served to

(11) Fischer, A. E.; Swain, G. M. *J. Electrochem. Soc.* **2005**, *152*, B369.
(12) Swope, V. M.; Sasaki, I.; Ay, A.; Swain, G. M. *ECS Trans.* **2007**, *3*, 27.
(13) Ay, A.; Swope, V. M.; Swain, G. M. *J. Electrochem. Soc.* **2008**, *155*, B1013.
(14) Fischer, A. E.; Lowe, M. A.; Swain, G. M. *J. Electrochem. Soc.* **2007**, *154*, K61.
(15) Swain, G. M. *J. Electrochem. Soc.* **1994**, *141*, 3382.
(16) DeClements, R.; Swain, G. M. *J. Electrochem. Soc.* **1997**, *144*, 856.
(17) Wang, J.; Swain, G. M. *Electrochem. Solid-State Lett.* **2002**, *5*, E4.
(18) Wang, J.; Swain, G. M. *J. Electrochem. Soc.* **2003**, *150*, E24.
(19) John, P.; Lee, J.-K.; Anderson, M.; Gray, F.; Wilson, J. *Chem. Vap. Deposition* **2006**, *12*, 714.
(20) Lee, J.-K.; Anderson, M. W.; Gray, F. A.; John, P. *Diamond Relat. Mater.* **2007**, *16*, 701.

maintain the hydrogen surface termination and prohibit any surface reconstruction to an sp^2-bonded phase. The plasma was then extinguished and the sample further cooled to room temperature under an H_2/Ar flow for 10 min.

Characterization by Scanning Electron Microscopy, X-ray Diffraction, and Raman Spectroscopy. The morphology of the as-received and B-UNCD-GC powders was characterized by field-emission scanning electron microscopy (JSM-6300F, JEOL, Ltd., Tokyo, Japan). Some of the powder samples were sputter-coated with a thin layer of Au to improve the surface conductivity. This served to improve the image resolution. The crystallinity of the as-received powder and the diamond overlayer was probed by X-ray diffraction. Diffraction spectra were recorded during a 2θ scan from 20 to 100° on a Rikagu Rotaflex RTP300 RC instrument. X-rays at 1.540 Å were generated from a rotating Cu anode. The microstructure of the as-received and B-UNCD-GC powder was evaluated by Raman spectroscopy. The spectra were acquired at room temperature using a Spex 1250 spectrograph with a 600 grooves/mm holographic grating (Horiba Jobin-Yvon). Light from an argon ion laser (Melles Griot CV) at 514.5 nm was used for excitation. The power density was 1.4 kW/cm^2. The detector was a Symphony 2000 × 800 CCD (Horiba Jobin-Yvon) with a pixel size of 15 μm. For each measurement, the spectrograph was calibrated using the first-order diamond phonon peak at 1332 cm^{-1} recorded from a high-pressure, high-temperature (HPHT) grown single-crystalline diamond sample.

Electrical Conductivity. The electrical conductivity of the as-received and B-UNCD-GC powders was determined by measuring ohmic resistance of the sample when placed between two metal plates. A fixed amount of powder was placed in a glass tube. Electrical contact was made to the powder with metallic plates (0.11 cm^2) on both ends of the vertically oriented tube. The resistance was measured with a constant mass of 240 mg applied to the top contact. $I-V$ curves were generated by applying ±6, ±10, and ± 20 mA currents and recording the corresponding voltage drop. The conductivity, σ (S/cm), was calculated as

$$\sigma = 1/RA$$

where R is the measured resistance (Ω), l is the powder thickness (cm), and A is the cross-sectional area of the sample (cm^2).

Electrochemical Measurements. Electrochemical characterization of the as-received and B-UNCD-GC powders was performed using a pipet electrode [13]. Briefly, the working electrode was prepared by packing the powder into a sealed plastic pipet tip (#104 BioDot, Scientific Inc., Burton, MI). A copper wire was then pressed into contact with the powder sample and was secured in place with adhesive. The closed end of pipet tip was then cut with a fine blade to expose the powder. The geometric area of the exposed powder was ~0.002 cm^2. The currents reported herein are normalized to this area. All measurements were performed using CHI650a potentiostat (CH Instruments, Inc., Austin, TX) in a single compartment glass cell. A platinum gauze served as the counter electrode, and homemade Ag/AgCl electrode (3 M KCl, $E = -65$ mV vs SCE) was used as the reference. All solutions were deoxygenated by purging with N_2 for 30 min prior to a measurement.

Chemicals. All chemicals were reagent-grade quality or better, and used without additional purification. All solutions were prepared with ultrapure water from a Barnstead E-Pure purification system (18 MΩ-cm). The supporting electrolyte was 0.5 M H_2SO_4 (99.999%, Aldrich). All glassware was cleaned by washing in an ethanol/KOH bath, an alconox/ultrapure water bath, and rinsing with ultrapure water.

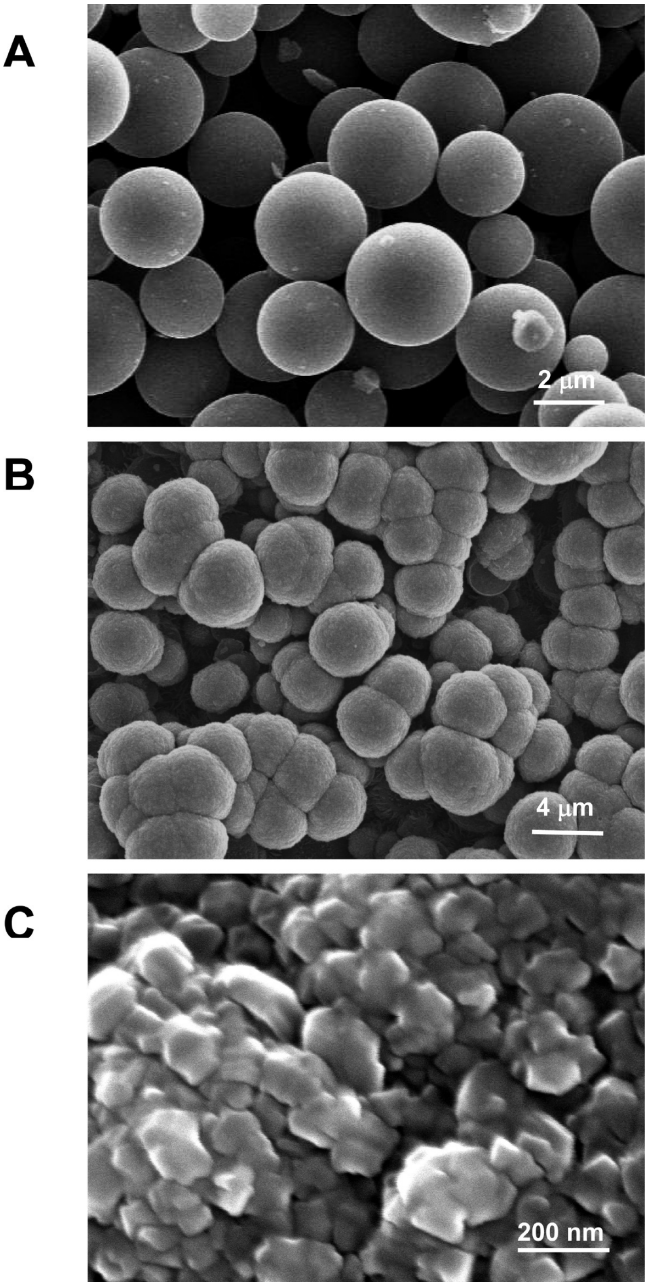

Figure 1. SEM images of (A) as-received and (B, C) B-UNCD-coated glassy carbon powder.

Results

Morphology and Microstructure of the B-UNCD-GC Powder. Scanning electron micrographs (SEM) of the as-received and B-UNCD-GC powders are presented in Figure 1A-C. The as-received powder has a spherical shape and a nominal diameter of 4 μm. The surface morphology is quite smooth with little or no porosity. Because the particles are smooth, it was easy to distinguish the rougher diamond overlayer. The surface morphology of the B-UNCD-GC particles after a 2 h growth is rougher than that of the as-received powder and is composed of nodular collections of diamond grains.

The nodules are 50−100 nm in dimension. This surface morphology is characteristic of UNCD[14,21−26]. It can be seen (Figure 1B) that there is some aggregation of neighboring particles (so-called particle fusion) as the diamond overlayer forms over multiple particles covalently attaching them together, rather than coating only individual particles. This serves to increase the electrical conductivity but also undesirably reduces the specific surface area of the material. Importantly, the images reveal that most of the GC powder surfaces get coated with UNCD. Within a sample, we typically found only a few particles that were incompletely coated (see image in Figure 4B). The contrasting morphologies of the as-received and UNCD-coated powders made this assessment rather straightforward. The higher-magnification image (Figure 1C) reveals that the nodular features of the UNCD actually consist of small faceted crystallites that are 50 nm, or so, in size.

A key reason for depositing the diamond from an Ar-rich rather than a more traditional H_2-rich source gas mixture is the reduced rate of carbon gasification in the Ar-rich environment. Coating sp^2-bonded carbon materials with diamond using traditional H_2-rich gas mixtures can be a problem because of the high rate of gasification that occurs in the presence of atomic hydrogen. Coating the glassy carbon powder with diamond grown from a traditional CH_4/H_2 gas mixture would therefore certainly be challenging due to a significant mass loss via carbon gasification to CH_4 and C_2H_2. It is likely that much of the powder would be gasified before any deposition occurs. Negligible gasification occurs in the Ar-rich environment, as we have shown for UNCD-coated Toray carbon paper [14].

X-ray Diffraction Analysis and Raman Spectroscopy. Figure 2 shows X-ray diffraction (XRD) patterns for the glassy carbon powder (A) before (GC) and (B) after UNCD deposition (B-UNCD-GC) for 2-h. Broad reflections are seen for GC at 25.1° (002), 43.4° (100), 53.0° (004), and 79.0° (110). The most intense reflection is the (002) line, which is reflective of the interlayer spacing between the graphene sheets. On the basis of the 2θ line position of 25.1°, the calculated interlayer spacing, d, is 0.352 nm ($d = n\lambda/2\sin\theta$). This is larger than the interlayer spacing in graphite of 0.335 nm. The nominal crystallite dimensions in the c-axis (perpendicular to the graphene sheets, the so-called crystallite thickness) and a-axis (parallel to the graphene sheets, so-called crystallite size or width) directions can be calculated from the Sherrer equation (L_c, $L_a = K\lambda/\beta\cos\theta$), in which K is the shape parameter taken to be 0.9, λ is the X-ray wavelength (0.154 nm), β is the full width at half-maximum of the reflection in radians, and θ is one-half of the 2θ angle.[27] The (002) reflection is used to calculate L_c and the (100) reflection is used to calculate L_a. No correction for instrumental broadening was made as this contribution to the peak widths was small ranging from 0.144 to 0.221 over the 2θ range. The line widths (β) for the (002) and (100) reflections were 5.1 and 3.5°, respectively, leading to calculated values for L_c and L_a of 1.6 and 2.9 nm, respectively.

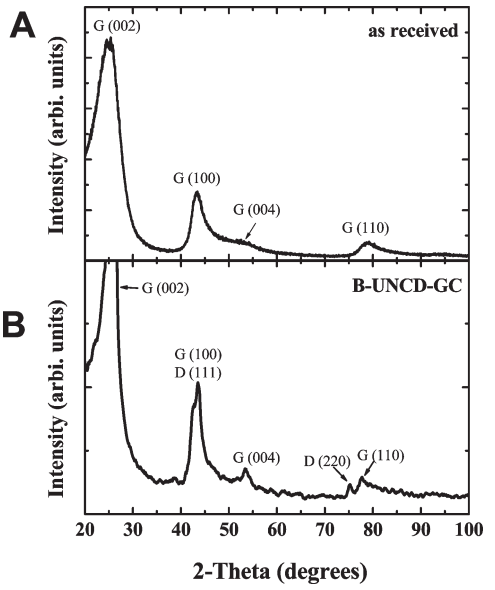

Figure 2. X-ray diffraction spectra of (A) as-received and (B) B-UNCD-coated glassy carbon powder.

The pattern for B-UNCD-GC is similar to that for the uncoated powder with the addition of two new reflections for cubic diamond at 43.6° (111) and 75.3° (220). The X-ray beam penetrates the diamond as well as the glassy carbon, so reflections from both materials are seen in the spectrum. Interestingly, there is a significant reduction in β for the glassy carbon (002) and (100) reflections to values of 1.4° and 1.8°, respectively. Although no statistical analysis was performed, the decreased line widths are consistent with increases in the glassy carbon L_c and L_a values after diamond deposition. It appears that the growth of crystalline diamond causes more microstructural ordering of the near-surface region of the underlying sp^2 carbon.

Figure 3 shows typical Raman spectra of the (A) as-received and (B) B-UNCD-GC powders after a 2-h deposition. The spectrum for the as-received powder has peaks at 1350 and 1580 cm^{-1}, which are the well-known D- and G-bands, respectively.[28−31] The broad peak at 1350 cm^{-1} represents a zone-edge A_{1g} mode that arises from disorder and the peak centered at 1580 cm^{-1} is an E_{2g} mode that is ascribed to the in-plane lattice phonon

(21) Show, Y.; Witek, M. A.; Sonthalia, P.; Swain, G. M. *Chem. Mater.* **2003**, *15*, 879.
(22) Gruen, D. M. *Annu. Rev. Mater. Sci.* **1999**, *29*, 211.
(23) Gruen, D. M. *MRS Bull.* **1998**, *23*, 32.
(24) Sumant, A. V.; Grierson, D. S.; Gerbi, J. E.; Carlisle, J. A.; Auciello, O.; Carpick, R. W. *Phys. Rev. B* **2007**, *76*, 235429.
(25) Birrell, J.; Gerbi, J. E.; Auciello, O.; Gibson, J. M.; Gruen, D. M.; Carlisle, J. A. *J. Appl. Phys.* **2003**, *93*, 5606.
(26) Butler, J. E.; Sumant, A. V. *Chem. Vap. Deposition* **2008**, *14*, 145.
(27) Cancado, L. G.; Talai, K.; Enoki, T.; Endo, M.; Kim, Y. A.; Mizusaki, H.; Jorio, A.; Coelho, L. N.; Magalhães-Paniago; Pimenta, M. A. *Appl. Phys. Lett.* **2006**, *88*, 163106.
(28) Nemanich, R. J.; Solin, S. A. *Phys. Rev. B* **1979**, *20*, 392.
(29) Tunistra, F.; Koenig, J. L. *J. Chem. Phys.* **1970**, *53*, 1126.
(30) Wang, Y.; Alsmeyer, D. C.; McCreery, R. L. *Chem. Mater.* **1990**, *2*, 557.
(31) Dennison, J. R.; Holtz, M.; Swain, G. M. *Spectroscopy* **1996**, *11*, 38.

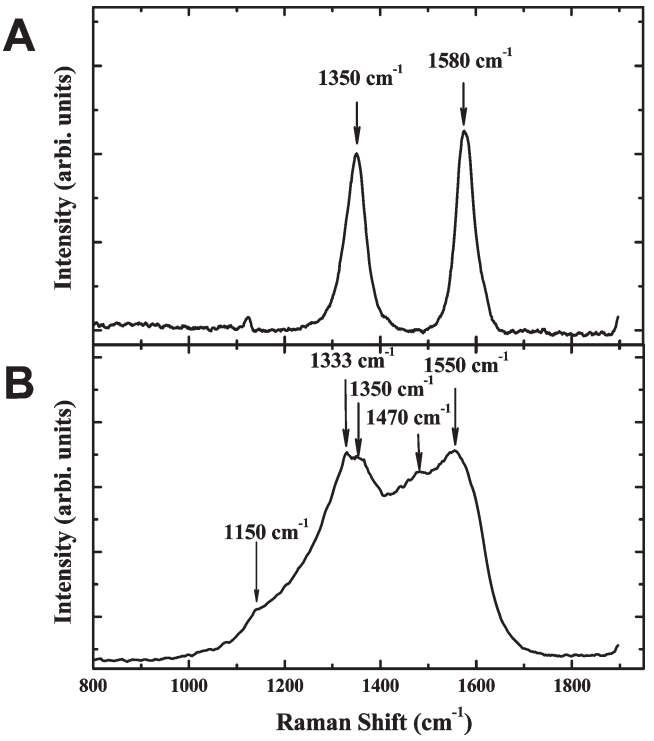

Figure 3. Visible Raman spectra of (A) as-received and (B) B-UNCD-coated glassy carbon powder.

of the graphitic domains within the material. The 1350 cm^{-1} mode becomes active when a carbon material possesses small crystallites or a high fraction of crystalline boundary. In other words, the 1350 cm^{-1} band tracks the fraction of edge plane or the degree of microstructural disorder. According to Tuinstra and Koenig, the D- and G-band intensity ratio (I_D/I_G) is inversely proportional to the effective crystallite size, L_a, in the direction of the graphite plane [29]. The ratio of 0.87 in the present spectrum is consistent with an L_a (e.g., crystallite size) of 5.5 nm. This is reasonably consistent with the 2.9 nm value determined from X-ray diffraction line width analysis. The Raman data, like the XRD data, confirm that the glassy carbon powder is microstructurally disordered with a high fraction of crystallite edges exposed because of a small crystallite domain size.

The Raman spectrum for B-UNCD-GC is quite distinct (Figure 3B). The Raman spectrum for microcrystalline diamond (not shown) consists of a single first-order phonon mode at 1333 cm^{-1}.[32,33] In contrast, the present spectrum has broad peaks at 1150, 1333, 1350, 1470, and 1550 cm^{-1}. These peaks are typical of boron-doped UNCD grown from Ar-rich source gas mixtures.[21−26,34−36] The Raman peak at 1333 cm^{-1} is assigned as the first-order phonon mode of diamond, and its peak width is much broader than that for microcrystalline diamond. This is, in part, due to the small diamond grain size (ca. 20−30 nm) in the film but also to the D-band scattering intensity at 1350 cm^{-1}. The presence of this D-band along with the G-band at 1550 cm^{-1} is consistent with some scattering being detected from the substrate carbon. It is also consistent the presence of the well-known presence of sp^2-bonded carbon in the grain boundaries of UNCD, carbon whose microstructure resembles than of *trans*-polyacetylene.[26,34−36] This peak is downshifted from the normal 1580 cm^{-1} position probably because of vibronic coupling between carbon atoms in a stronger sp^2-bonded configuration (aromatic) and carbon atoms in a weaker sp^3-bonding arrangement. The I_D/I_G ratio appears to be slightly less than 1.0, but it is difficult to determine given the convergence of the 1333 and 1350 cm^{-1} bands. Although it is possible that the 1350 and 1580 cm^{-1} bands result from the carbon of the underlying GC powder, it should be noted that this scattering intensity is always present for UNCD films (grown on noncarbon substrates) deposited from Ar-rich gas mixtures [26,34−36]. The peaks at 1150 and 1470 cm^{-1} are often used as a signature for high quality UNCD, but have been assigned to sp^2 C−H vibrational modes of *trans*-polyacetylene segments in the grain boundaries[26,34−36]. Even though the fraction of sp^2-bonded carbon in the film is low, the large Raman scattering cross-section for this carbon using visible excitation light (514.5 nm) causes the associated vibrational modes to dominate the spectrum.

Other Carbon Microstructures Formed. Although SEM images routinely revealed that most of the GC powder particles in a sample were fully covered by UNCD, some incompletely coated particles were sometimes found. It is difficult to approximate the percentage of such particles but 10% seems in order. An example is shown in Figure 4A and B. The incomplete coverage is likely due to inhibited transport of reactive species to the surface, which slows the growth rate. For instance, these particles may have been directly contacting the Si substrate or could have been buried within the powder sample during the deposition run. Both would result in inhibited mass transport of gaseous reactants and incomplete coverage. The images are useful because they provide an idea of the UNCD coating thickness, which appears to range from 100 to 500 nm. Closer inspection of the single particle shown in Figure 4B reveals some interesting surface morphological features. Ridgelike structures are seen on the underlying GC powder surface and it is on these ridges that the diamond nuclei form (see arrows in Figure 4A and higher mag. image in Figure 4B). These ridgelike features are identical to those previously reported for GC plates treated in a hydrogen plasma (so-called hydrogenated glassy carbon).[37−39] In that work, a mechanism was proposed whereby atomic hydrogen chemisorbs at the graphitic edge plane sites progressively converting the aromatic C−C bonding to alicyclic hydrocarbons (e.g., cyclohexane). This is followed by final ring-opening

(32) Solin, S. A.; Ramdas, A. K. *Phys. Rev. B* **1970**, *1*, 1687.
(33) Mermoux, M.; Marcus, B.; Swain, G. M.; Butler, J. E. *J. Phys. Chem. B* **2002**, *106*, 10816.
(34) Ferrari, A. C.; Robertson, J. *Phys. Rev. B* **2001**, *63*, 121405.
(35) Birrell, J.; Gerbi, J. E.; Auciello, O.; Gibson, J. M.; Johnson, J.; Carlisle, J. A. *Diamond Relat. Mater.* **2005**, *14*, 86.
(36) Arenal, R.; Montagnac, G.; Bruno, P.; Gruen, D. M. *Phys. Rev. B* **2007**, *76*, 245316.
(37) DeClements, R.; Swain, G. M.; Dallas, T.; Holtz, M. W.; Herrick, R. D.II; Stickney, J. L. *Langmuir* **1996**, *12*, 6578.
(38) Chen, Q.; Swain, G. M. *Langmuir* **1998**, *14*, 7017.
(39) Kuo, T.-C.; McCreery, R. L. *Anal. Chem.* **1999**, *71*, 1553.

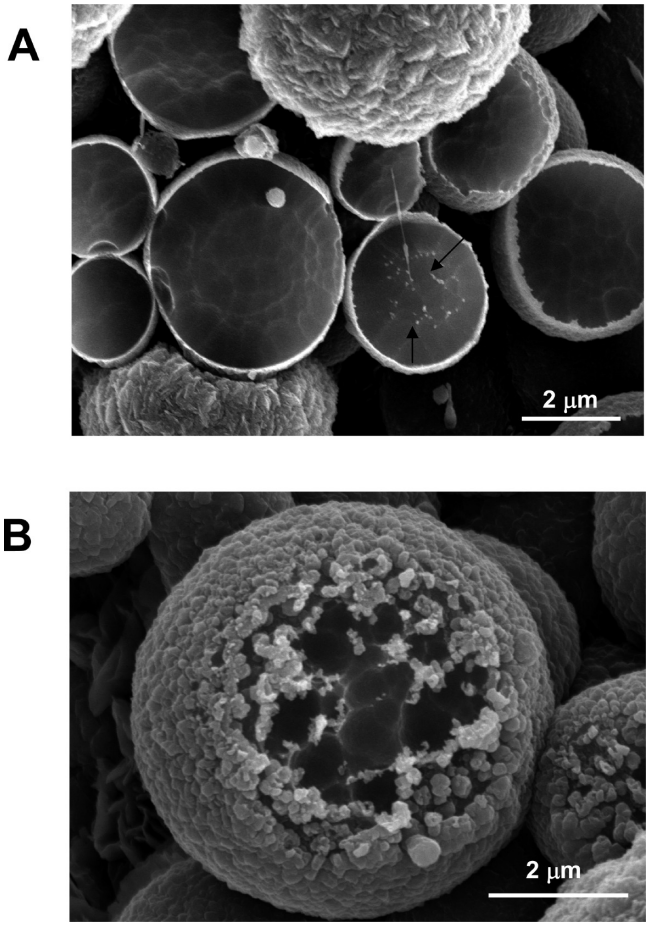

Figure 4. SEM images of B-UNCD-coated glassy carbon particles revealing (A) incomplete diamond growth and (B) nucleation of nanocrystalline diamond at ridgelike features on the glassy carbon surface. These ridgelike features are the result from the initial hydrogenation of the surface.

hydrogen addition reactions to produce aliphatic moieties[38]. The hydrogenation reactions, prior to any gasification, convert the surface carbon atoms into an sp^3-bonded diamond structure. It is on this surface that diamond readily nucleates and grows. Mehandru et al.[40] and Lambrecht et al.[41] reported computational work showing the structure and energetics of the sequential addition of hydrogen atoms to the extended edge of a graphene sheet. The progressive hydrogenation transforms the aromatic rings to their saturated analogues. Their results showed that hydrogen atoms can chemisorb to a graphite sheet far from the edge causing distortion from a planar to a tetrahedral structure for the carbon atoms to which they are bound.

There were also other regions in a sample where nanocrystalline graphite platelets were observed. SEM images showing this microstructure are presented in Figure 5A and B. Raman spectra were used to confirm that the platelet microstructure is indeed nanocrystalline graphite with a high fraction of exposed crystallite edges. A representative spectrum is presented in Figure 5C, which shows a broad peak at 1360 cm^{-1} (D-band) that

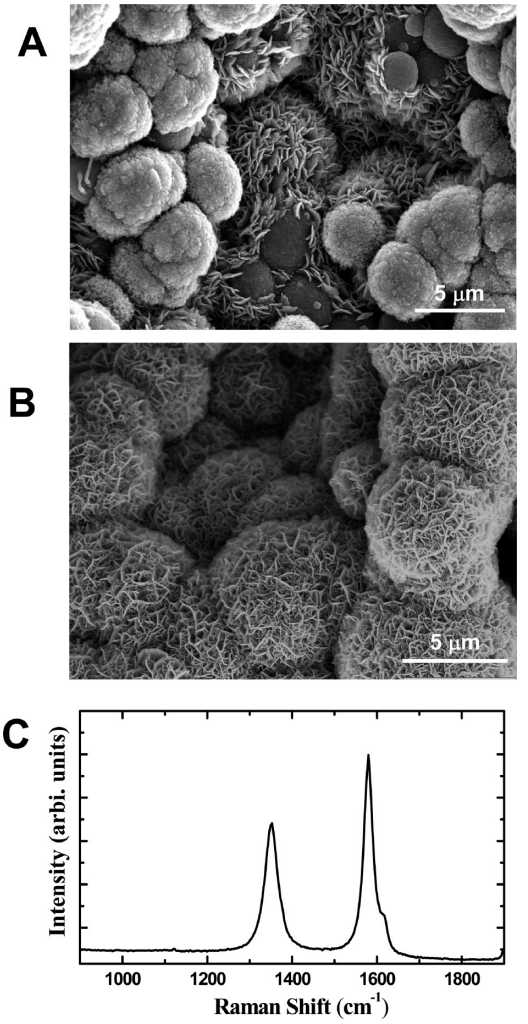

Figure 5. SEM images of B-UNCD-coated glassy carbon particles revealing (A) the nodular morphology of the UNCD along with a codeposited platelet-like nanocrystalline graphite, (B) preferential growth of the platelet nanocrystalline graphite using 3% CH_4 in the source gas, and (C) a Raman spectrum of platelet structure confirming that it is nanocrystalline graphite.

is associated with the high fraction of exposed crystallite boundaries and the 1580 cm^{-1} peak (G-band) assigned to the first-order phonon mode for graphite [28−33]. There is also a small peak at 1625 cm^{-1}, which we tentatively assign to reduced symmetry of the nanocrystalline graphite impurity due to boron insertion during its formation [30]. The platelets appear to be oriented predominantly with their graphene sheets normal to the GC powder surface. In other words, there is a high fraction of crystallite boundary or edge exposed. The platelets are on the order of 100−200 nm thick and 600−1000 nm wide. The I_D/I_G intensity ratio is 0.68. According to work by Tunistra and Koenig, this ratio corresponds to crystallite size, L_a, of ~7 nm[29]. On the basis of this result, the platelets appear to consist of smaller, randomly ordered graphitic crystallites. Morphologically and microstructurally similar diamond/carbon nanoflakes have been formed on silica spheres using variable gas-phase CVD growth chemistries [42].

(40) Mehandru, S. P.; Anderson, A. B.; Angus, J. C. *J. Phys. Chem.* **1992**, *96*, 10978.
(41) Lambrecht, W. R. L.; Lee, C. H.; Segall, B.; Angus, J. C.; Li, Z.; Sunkara, M. *Nature (London)* **1993**, *364*, 607.
(42) Lee, J.-K.; John, P.; Kim, S.-C.; Lee, W.-S.; Wilson, J. I. B. *Diamond Relat. Mater.* **2008**, *17*, 1216.

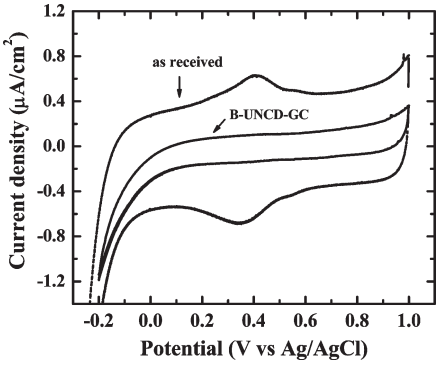

Figure 6. Cyclic voltammetric $i-E$ curves for as-received and B-UNCD-coated glassy carbon powder after 20 continuous scans in 0.5 M H_2SO_4.

Electrochemical Characterization. Cyclic voltammetric $i-E$ curves were recorded for the as-received and B-UNCD-GC powders in 0.5 M H_2SO_4. Figure 6 shows representative curves for both powders after 20 cycles between −0.3 and 1.0 V vs Ag/AgCl reference electrode. The currents were normalized to the geometric area of the pipet electrode (~0.002 cm^2). The current density for the B-UNCD-GC powder is 3−5 times lower than that for the as-received powder. Furthermore, the curve for the diamond-coated sample is featureless while well resolved peaks are seen in the curve for the as-received powder centered at 0.39 V. These currents are associated with the oxidation and subsequent reduction of hydroquinone functional groups that form at the edge plane sites of the graphitic domains[43−45]. The diamond-coated surface has none of this reactive, sp^2-bonded edge plane carbon so this redox couple does not form. The lower background current for the B-UNCD-coated powder is due to a lower double layer capacitance for diamond (ca. 5−10 $\mu F/cm^2$ vs 25−30 $\mu F/cm^2$ for glassy carbon), and a reduced pseudocapacitance because of comparatively low levels of redox-active and or ionizable C−O functional groups.[14,37−39,43−45] The diamond surface can easily be oxidized (e.g., OH formation) but the surface functionalities that form are not redox-active in this potential range.

Evaluation of Microstructural and Dimensional Stability. To be a viable electrocatalyst support for PEM fuel cells, the carbon material should possess high electrical conductivity, high specific surface area, and superb durability. The microstructural and dimensional stability of the as-received and B-UNCD-GC powders were evaluated after anodic polarization at 1.6 V vs Ag/AgCl in 0.5 M H_2SO_4 (25 °C) for 30 min. Figure 7 shows the continuous amperometric $i-t$ curves for the two powders. The current was normalized by the geometric area of the pipet electrode (~0.002 cm^2). The polarization measurements were performed twice for each sample and the charge density passed for the as-received powder was significantly greater (1.41 and 2.03 C/cm^2) than that for the B-UNCD-GC powder (0.28 and 0.49 C/cm^2). For the B-UNCD-GC powder, the current density decreased rapidly after the potential application reaching a more or less constant current density of ca. 100 $\mu A/cm^2$ for most of the polarization period. On the other hand, the current for the as-received powder decreased during the first 50 s of the polarization but was followed by second increase to a near constant current density of ca. 400 $\mu A/cm^2$ for the remainder of the polarization period. The higher current density for the as-received powder is consistent with more extensive oxidation of this surface as compared to the diamond-coated surface.

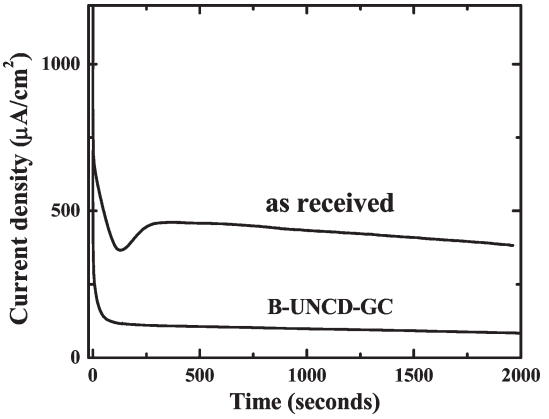

Figure 7. Continuous amperometric $i-t$ curves for as-received and B-UNCD-coated glassy carbon powder recorded during anodic polarization at 1.6 V vs Ag/AgCl for 30 min in 0.5 M H_2SO_4. Temperature 80 °C. The currents are normalized to the area of the electrode contacting the supporting electrolyte solution.

Morphology and Microstructure after Anodic Polarization. The larger charge density for the as-received powder indicates that more extensive oxidation of the material occurs. To learn if the oxidation involves microstructural alterations and carbon corrosion, SEM images were obtained. SEM images of the two powders before and after anodic polarization are shown in Figure 8A−D. The images indicate that indeed microstructural degradation and carbon corrosion occurred. A large number of fractured spheres are evident (e.g., see broken particles in the center of the image) with greatly reduced diameters (Figure 8B). In contrast, there is no apparent degradation of the B-UNCD-GC powder after polarization (Figure 8C and D), as there is no evidence for particle fracturing or pitting. Undoubtedly, some of the uncoated powder particles will degrade under these polarization conditions, but these powder particles constitute a very low percentage of the total sample so no damaged particles are readily observable. However, in other images of incompletely coated particles, we found that small pits developed because of carbon corrosion at the uncoated sp^2 carbon sites (data not shown). Also, the nanocrystalline graphite platelets appear to be gasified as they were more difficult to locate in samples that had been polarized.

Discussion

The structure of glassy carbon has been the subject of research since the 1960s when it was first produced. The most widely accepted model is that put forward by

(43) Kinoshita, K.; Bett, J. *Carbon* **1988**, *12*, 71.
(44) Fagan, D. T.; Hu, I. F.; Kuwana, T. *Anal. Chem.* **1985**, *57*, 2759.
(45) Hu, I. F.; Karweik, D H.; Kuwana, T. *J. Electroanal. Chem.* **1985**, *188*, 59.

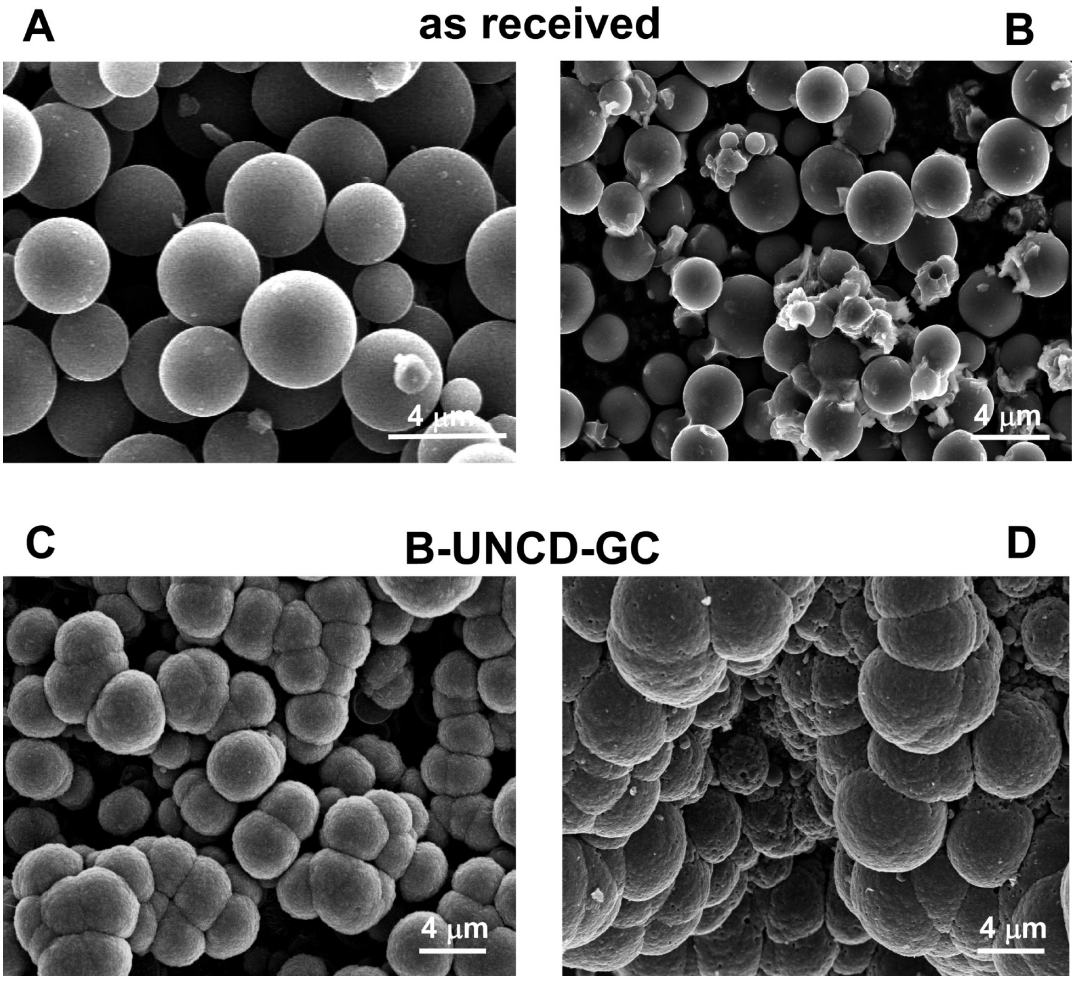

Figure 8. SEM images of GC powder as-received (A) before and (B) after polarization at 1.6 V vs Ag/AgCl for 30 min in 0.5 M H_2SO_4. Temperature 80 °C. Images are also shown of B-UNCD-coated GC powder (C) before and (D) after the same polarization.

Jenkins and Kawamura.[46] The material is believed to contain mostly sp^2-bonded carbon with the short-range order of a strained graphite-like layer.[46,47] The structure has been proposed to bear some resemblance to the linear polymeric precursor the material is prepared from consisting of very narrow curved and twisted ribbons of graphitic carbon.[47] The long ribbons of multiple, stacked graphene sheets twist, bend and interlock with each other. More recently, it has been proposed that the microstructure actually consists of broken or imperfect fullerene-related nanoparticles [48]. Regardless, the material is microstructurally disordered with small, nanometer-sized graphitic domains. The material has a high fraction of exposed edge plane and the carbon atoms at these crystallite edges are much more reactive than in-plane carbon atoms. Glassy carbon generally has low gas permeability because of the interlocking structure and the absence of porosity. However, glassy carbon is susceptible to microstructural damage and corrosion during electrochemical oxidation. Taken together, the data presented herein reveal that coating the glassy carbon particles with a boron-doped UNCD overlayer (100−500 nm thick) imparts a high degree of dimensional stability and corrosion resistance to the material. This same approach could be used to modify other powderous materials in order to improve their dimensional stability and corrosion resistance. Even though having the substrate powders spread across the CVD reactor stage is not the optimum arrangement for depositing diamond on their surfaces because of mass transfer limitations and limited sample size, most of the GC particles were covered with an UNCD layer. SEM images, XRD analysis, and Raman spectroscopy confirmed the presence of UNCD layer on the GC surface. Furthermore, Raman spectroscopy revealed that the UNCD layer is composed of aggregated grains of cubic diamond (the aggregates are 50−100 nm in dimension) with sp^2-bonded carbon in the grain boundaries. Some of this grain boundary carbon consists of transpolyacetylene segments, according to Ferrari and Robertson,[34] and according to our results, some of this carbon is nanocrystalline graphite (e.g., glassy carbon-like). The fraction of the total carbon in the film that is in an sp^2-bonding configuration is low and yet the Raman spectrum is dominated by the vibrational modes associated with this carbon. This is because the scattering cross-section for sp^2 carbon (graphite

(46) Jenkins, G. M.; Kawamura, K. *Nature* **1971**, *231*, 175.
(47) Harris, P. J. F. *Critical Rev. Solid-State Mater. Sci.* **2005**, *30*, 235.
(48) Harris, P. J. F. *Philos. Mag., A* **2004**, *84*, 3159.

as the model) is ca. 50× larger that the cross-section for diamond [49,50]. Even with the sp^2 carbon impurity in the grain boundaries, the UNCD overlayer exhibits excellent dimensional stability and corrosion resistance. In other words, the presence of the sp^2 carbon impurity carbon does not compromise the level of protection provided by the diamond overlayer.

Our results further indicate that UNCD readily nucleates and grows on the GC surface. It appears that the initial step in the diamond nucleation and growth process involves hydrogenation of the GC graphite edge planes to produce an sp^3 diamond-like surface microstructure. The hydrogenation distorts the lattice and causes ridge-like features to form. It is on these ridges that the initial diamond nucleation and growth occurs. Also, the growth of diamond causes microstructural ordering in the near-surface region of the glassy carbon, as evidenced by Raman data. The layer forms continuously over most of the powder particle surfaces and there is some particle aggregation due to diamond overlayer formation over neighboring particles. This aggregation probably improves the electrical conductivity but undesirably reduces the specific surface area of the material. Additionally, because of a combination of higher reactive carbon concentrations and temperatures locally within a powder sample, nanocrystalline graphite platelets form. These platelets are on the order of 100−200 nm thick and 600−1000 nm wide. They predominately form with the graphene sheets oriented normal to the surface. Other work in our group has shown that when the CH_4/H_2−Ar volume percentage reaches the 3% level, then these graphite platelets predominately form during diamond deposition.

Deposition of UNCD is attractive for modifying powderous sp^2 carbon materials because of the minimal gasification that occurs in the Ar-rich source gas. In more traditional CH_4/H_2 source gas mixtures, significant sp^2 carbon substrate mass loss would occur because of gasification by atomic hydrogen. Gasification can quickly become catastrophic to small-sized sp^2 carbon materials.

The continuous amperometric $i-t$ curves along with the postpolarization SEM images indicate that electrochemical oxidation of the as-received powder involves surface oxide formation, as well as layer plane exfoliation and fracturing due to the stresses of the oxide formed and or the oxidation of intercalation compounds. This is followed by carbon corrosion. The $i-t$ curve has an initial decrease in the current density and then a second increase at about the 50 s time point. The initial current density decay is associated with double layer charging, possibly some minor anion intercalation (HSO_4^- or SO_4^{2-}), and surface oxide formation at the edge plane sites. After the 50 s period, the intercalation and oxide stress presumably cause layer plane exfoliation and fracturing. This produces new reactive edge plane and increases the surface area in contact with the solution, hence the current density increases. At some point during the polarization, mass loss due to carbon corrosion occurs. When coated with B-UNCD, the current density during anodic polarization is less, and more importantly, the coating protects the GC powder from microstructural degradation and corrosion.

Conclusions

It was demonstrated that the microstructural stability and corrosion resistance of glassy carbon powder can be significantly improved by overcoating the material with a thin layer of boron-doped UNCD. UNCD readily nucleates and grows on the glassy carbon surface without any seeding or pretreatment, but the initial nucleation appears to occur on a hydrogenated, diamond-like carbon surface. Little gasification of the glassy carbon occurs in the Ar-rich gas environment. Even though the reactor design used was not optimum for coating powders, most of the powder sample was coated with B-UNCD. There was some aggregation due to growth of the diamond overlayer on multiple neighboring particles. Because of mass transport limitations, some regions of a sample were found where incomplete diamond coverage was observed. Additionally, because of local variations in temperature and reactive carbon level within the powder sample, small amounts of nanocrystalline graphite form on some regions of the powder surface. Future work will involve refinements of the CVD deposition system to enable more uniform deposition over powder surfaces.

Acknowledgment. This work was sponsored by the Chemical Sciences, Geosciences and Biosciences Division, Office of Basic Energy Sciences, Office of Science, U.S. Department of Energy (DE-FG03-95ER14577). We thank Lesia Protsailo from UTC Power Corp. for her contribution to this work.

(49) Knight, D. S.; White, W. B. *J. Mater. Res.* **1989**, *4*, 385.
(50) Wagner, J.; Wild, C.; Koidl, P. *Appl. Phys. Lett.* **1991**, *59*, 779.